Institut für Photovoltaik

Institute for Photovoltaics

Universität Stuttgart

Jahresbericht 2013

Annual Report 2014

Jahresbericht
Annual Report

2013
2014

Redaktion • edited by

Jürgen R. Köhler
Jürgen H. Werner
grafik-service@web.de

Vorwort

Liebe Freunde des *ipv*,

Das Institut für Photovoltaik hat zwei schwierige Jahre durchlaufen, die schwierigsten in den letzten 30 Jahren. Eine Negativmeldung nach der andern über die Photovoltaik und andere Arten der Erneuerbaren Energien ging durch die Presse, Firmen und Fördermittel brachen weg – drei Jahre nach der Reaktorkatastrophe von Fukushima. Die Situation dreht sich derzeit wieder und langsam wächst eine fast triviale Erkenntnis: Wie bitte sollte man die Energiewende ohne Photovoltaik hinbekommen? Schon heute ist in Süddeutschland Photovoltaikstrom mit 8 cent/kWh billiger als Strom aus jedem Kohle- oder Gaskraftwerk. Und das Totschlagargument „Speicherung“ verfängt schon eine Weile nicht mehr. Gespeicherter Strom ist heute schon bis herunter zu 15 cent/kWh zu haben. Zusammen mit der Photovoltaik ist er damit billiger als Strom „aus der Steckdose“.

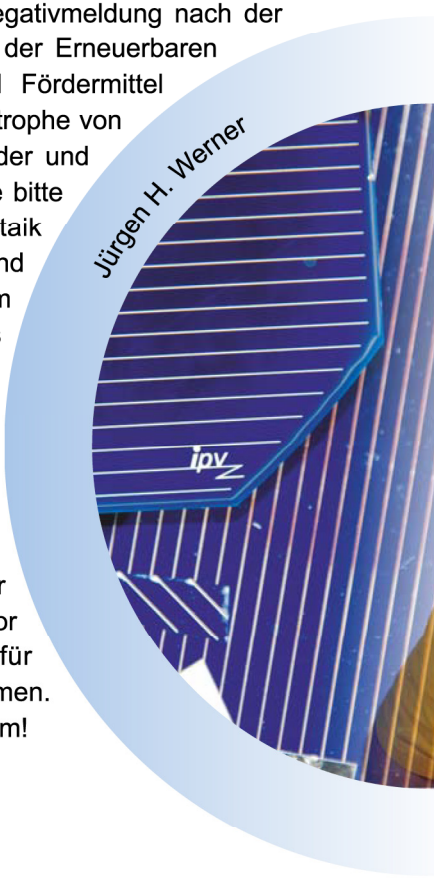

Auch das *ipv* widmet sich in Zukunft noch mehr der Speicherung: In wenigen Tagen wird Professor Peter Birke hier am Institut die Professur für „Elektrische Energiespeichersysteme“ übernehmen. Wir freuen uns alle auf die Zusammenarbeit mit ihm!

Stuttgart, Dezember 2014

J. Werner

Jürgen H. Werner

Preface

Dear friends of the *ipv*,

The Institute for Photovoltaics endured two difficult years, the most difficult ones in the past 30 years. A series of negative reports about solar energy and other types of renewable energies appeared in the newspapers, companies collapsed and funding ceased – three years after Fukushima. The situation is now changing for the better and slowly the almost trivial insight is growing: how could the transformation of the energy system possibly work without photovoltaics? In Southern Germany, already today photovoltaic electricity, costing 8 cent/kWh, is cheaper than electricity from any gas or coal power station. And the knock-out argument "storage" has meanwhile become obsolete. Stored electricity is available nowadays for 15 cent/kWh. Together with solar electricity it is hence cheaper than electricity "from the socket".

The *ipv* too is going to put even more focus on storage. In a few days, Prof. Peter Birke will assume the professorship for Electrical Energy Storage Systems here at the institute. We are all looking forward to collaborating with him!

Stuttgart, December 2014

J. Werner

Jürgen H. Werner


IPV

Inhaltsverzeichnis • Table of Contents

Mitarbeiter
People

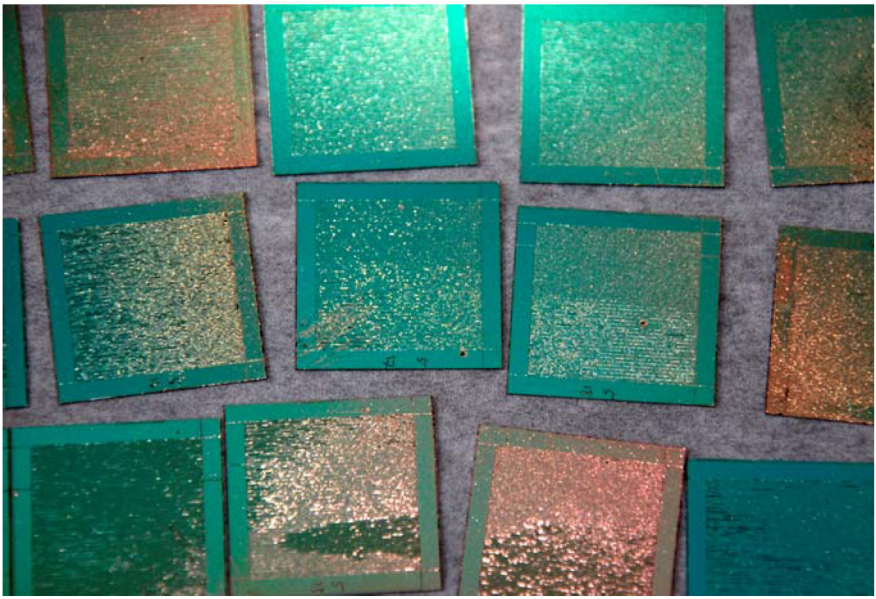

Forschung

Solarzellen

Photovoltaik-Systeme

Mikro - und Optoelektronik

Energie

Lehre

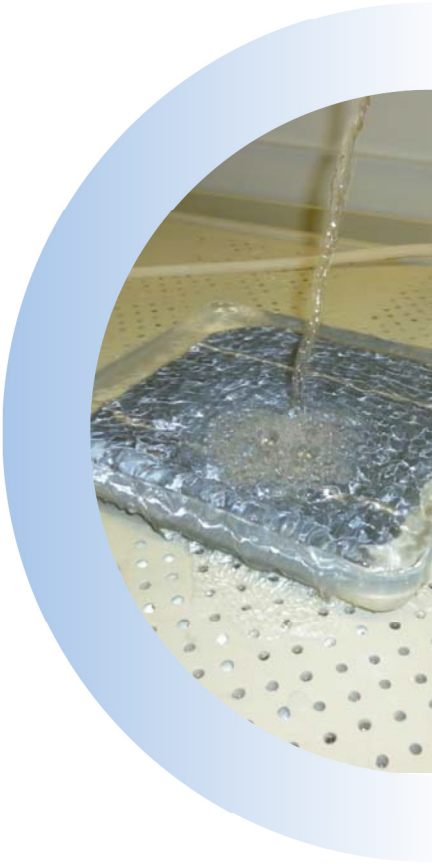

Institutsleitung • Head of the Institute

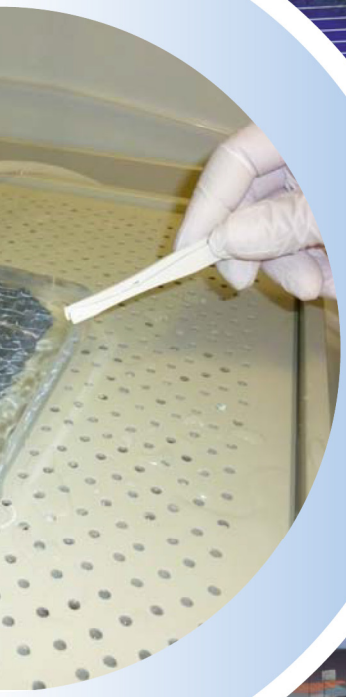

Verwaltung • Administration

Gruppe Laserprozesse
Group Laser Processing

(Gruppenleiter / Group Leader: Jürgen R. Köhler)

Die Gruppe „Laserprozesse“ entwickelt neue Technologien zum Laserprozessieren von Materialien für die Elektrotechnik. Neben dem Laser-Prozessieren kristalliner Silizium-Scheiben für Solarzellen und Halbleiterbauelemente bildet die Herstellung poröser Anoden aus Silizium für Lithium-Ionen Batterien einen weiteren Schwerpunkt. Im Vordergrund unserer Arbeiten stehen die Weiterentwicklung unseres Laserdotier-Prozesses für rückseitenkontaktierte Hocheffizienz-Solarzellen, die laserunterstützte Feinlinienmetallisierung, die Ablation dielektrischer Schichten, das Aufschmelzen und Durchdotieren von Silizium Wafern für Halbleiterbauelemente sowie das Laser-Porosieren gesputterter und mit PECVD abgeschiedener Silizium-Schichten. In enger Zusammenarbeit mit der Gruppe „Industrielle Solarzellen“ sowie der „Technologiegruppe“ am *ipv* optimieren wir unsere Laser-Prozesse zur Herstellung hocheffizienter, rückseitenkontaktierter Solarzellen mit einem Wirkungsgrad von über 23,5 %.

The “Laser Processing” group explores new technologies for laser processing of materials for electrical engineering applications. Porous anodes for lithium ion batteries are a new focus of our research, besides laser-processing of crystalline silicon wafers for solar cells and semiconductor components. The main topics of our research work are pulsed laser doping for high efficiency back-contact solar cells, the ablation of dielectric layers, melting- and doping-through of silicon wafers for semiconductor elements as well as laser porification of sputtered and PECVD silicon layers. A close collaboration with the research groups “industrial solar cells” and “technology” at *ipv* optimizes our laser processes for the fabrication of high efficiency back-contact solar cells with efficiencies above 23.5 %.

Gruppe Technologie
Group Technology

(Gruppenleiterin / Group Leader: Birgitt Winter)

Die Gruppe „Technologie“ setzt sich aus den technischen Mitarbeitern des Instituts zusammen. Sie betreut die gesamte Infrastruktur des Instituts. Die konstante Zusammensetzung der Gruppe in den letzten beiden Jahren hat uns erstmals ermöglicht, die Aufgabenvielfalt jedes Einzelnen weiter auszuweiten. Das bietet uns die Basis, den neuen Anforderungen gerecht zu werden, die durch die laufenden Projekte am *ipv* entstehen. Zu unseren Kompetenzen gehören Oxidationen, Diffusionen, Plasmadepositionen, nasschemische Reinigung und Ätzen, Lithographie, Metallisierung und vieles andere mehr. Unser Ziel ist eine gute Reproduzierbarkeit von Prozessen durch die Entwicklung von standardisierten Prozessabläufen und Qualitätskontrollstandards.

The group “Technology” is composed of the technical staff of *ipv* and supervises the entire infrastructure of the institute. The constant composition of the group in the last two years allows us, for the first time, to further expand the variety of tasks of each individual. This provides us with the basis to meet the new challenges that arise on *ipv* through ongoing projects. Our capabilities include oxidation, diffusion, plasma deposition, wet chemical cleaning and etching, lithography, metallization and much more. Our aim is a high reproducibility of all processes by developing standardized process flows and quality control standards.

Gruppe Sensorik
Group Sensor Technology

(Gruppenleiter / Group Leader: Markus Schubert)

Die Arbeitsgruppe „Sensorik“ nutzt dünne Siliziumschichten zur Entwicklung hochempfindlicher Photodetektoren und poröser Si-Anoden für Lithium-Ionen-Batterien. Wir entwickeln und erproben neuartige Messmethoden zur Charakterisierung von Photovoltaiksystemen und -modulen. Außerdem begleiten wir den Praxistest eines elektrischen Quartierspeichers im Landesprojekt STROMBANK mit Messtechnik, Datenauswertung und Modellierung. Die speziellen Photodetektoren zur Überwachung der Medikamentierung von Patienten nach Organtransplantationen entstehen im EU-Verbund NANODEM in enger Zusammenarbeit mit dem Institut für Physikalische und Theoretische Chemie der Universität Tübingen. Die übrigen Themen bearbeiten wir mit verschiedenen Partnern in Industrie und Forschungseinrichtungen.

The “Sensor Technology” work group at *ipv* uses thin film silicon for developing high-sensitivity photodetectors and porous Si anodes for lithium ion batteries. We develop and test novel characterization techniques for photovoltaic systems and modules. Another task monitors the integration of a battery container into the electricity grid of a housing district by data acquisition, analysis and modelling. The high-sensitivity photodetectors are specifically designed for therapeutic drug monitoring in patients after organ transplantation during the EU project NANODEM and a close cooperation with the Department of Analytical Chemistry at the University of Tübingen. On the other tasks, we cooperate with various partners from industry and research institutes.

Gruppe Industrielle Solarzellen
Group Industrial Solar Cells

(Gruppenleiterin / Group Leader: Renate Zapf-Gottwick)

Der Schwerpunkt der Forschungsaktivitäten der Gruppe „Industrielle Solarzellen“ liegt auf Prozessen, die den Wirkungsgrad und die Herstellkosten von kristallinen Silizium-Solarzellen verbessern. Hier arbeiten wir z.B. am Ersetzen des teuren Metalls Silbers für die Metallisierung. Außerdem beschäftigen wir uns zusammen mit der Gruppe „Laserprozesse“ mit rückseitenkontaktierten Solarzellen, die durch Laserprozesse sehr kostengünstig und schnell produziert werden können. Auf kleiner Fläche von 4 cm^2 haben wir bereits einen Wirkungsgrad von 23,5 % erreicht. Jetzt erfolgt das Hochskalieren und die Umsetzung der Prozesse auf eine Fläche von 12,5x12,5 cm^2 in enger Zusammenarbeit mit der Gruppe „Technologie“. Ein weiteres Projekt zielt auf Photovoltaik-Module, die das Ende ihrer Lebenszeit erreicht haben. In einer worst-case Studie haben wir bereits gezeigt, dass Blei und Cadmium aus den Modulen austreten können. Jetzt klären wir, wie die Wege und Mechanismen der Schadstofffreisetzung sind.

Our group “Industrial Solar Cells” is engaged in different research activities for improved efficiencies and production costs of industrial solar cells. For example, we replace silver for their metallization. Together with the *ipv*-group “Laser Processing”, we work on laser processed backside contacted solar cells. On the area of 4 cm^2, we showed the proof-of-concept by an efficiency of 23.5 %. Now, in close cooperation with the group “Technology”, we scale up all processes to an area of 12.5x12.5 cm^2. Another project aims at photovoltaic modules, which reached the end of their lifetime. Our worst case study already showed that harmful substances are released, mainly lead and cadmium. Now, we identify the ways and mechanisms for the leaching out of harmful substances from modules.

einkristallines

mikrokristallines

Silizium

nanokristallines

amorphes

Wissenschaftliche Beiträge
Scientific Contributions

Publikationen
Publications

Laser Processed Thin Film Silicon Anodes for Lithium-Ion-Batteries

Author: C. Sämann
*In collaboration with: J. R. Köhler, M. B. Schubert, M. Wachtler**

Silicon has the highest storage capacity for lithium and is therefore a promising candidate for anodes in next-generation batteries. Based on a filed patent, the *ipv* developed a process to produce porous thin film silicon by pulsed laser irradiation. In collaboration with the Centre for Solar Energy and Hydrogen Research (ZSW) Ulm porous thin film silicon on metal foil substrates are successfully tested by galvanostatic measurements in lithium half-cells. The silicon anodes show cyclic stability over more than 300 cycles at 2C with a reversible capacity above 950 mAh/g.

Figure 1 shows a scanning electron microscope (SEM) picture of a 300 nm thick sputtered silicon layer, treated by single line shaped laser pulses of wavelength λ = 532 nm. A comparison of the laser treated areas with the as-deposited silicon in between the pulses demonstrates the large increase of the surface area after laser irradiation. Silicon absorbs the energy of the laser pulse, resulting in a phase change from solid to liquid. Incorporated argon atoms leave the liquid thin film as small gas bubbles creating pores in a diameter between 60 nm and 1.5 µm. The diameter increases with increasing energy density of the laser pulse.

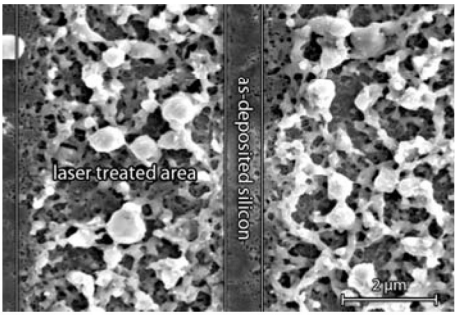

Figure 1:
SEM picture of sputtered silicon after pulsed laser irradiation with a line shaped laser focus of wavelength λ = 532 nm. The laser treated area contains many pores in contrast to the as-deposited silicon in between the pulses.

*(*ZSW Ulm)*

Figure 2 shows results of the galvanostatic cycling of a porous silicon thin film on stainless steel substrate as anode in a lithium half-cell. Charging is limited to a charge capacity of 1000 mAh/g. After the typical initial capacity losses, the anode shows a stable discharge capacity of more than 950 mAh/g at a current rate of 2C. Irreversible capacities by side reactions of silicon and the electrolyte, as well as volume expansion induced mechanical fracture and delamination of silicon from the substrate, are probable reasons for the difference between charge and discharge capacity. Future research will focus on minimizing irreversible capacities and increasing the silicon film thickness.

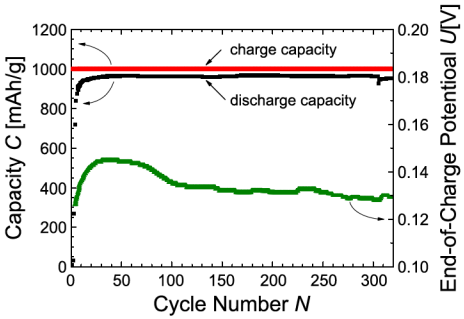

Figure 2:
Galvanostatic measurements of porous silicon thin film with (39 µg/cm^2) in 1 M LiPF6 / EC:DMC (1:1) on stainless steel foil substrates at ZSW Ulm. Charge capacity is limited to 1000 mAh/g. Silicon anode shows stable cycling performance over more than 300 cycles.

Thin Film Silicon for Flexible Metal-Air Batteries

Author: A. Garamoun
In collaboration with: M. Schubert, J. H. Werner

Due to its high energy density, theoretical studies propose silicon as a promising candidate material for metal-air batteries. This work, for the first time, reports on experimental results using n-type doped amorphous silicon and silicon carbide as fuel in Si-air batteries. Thin film silicon is particularly interesting for flexible and rolled batteries with high specific energies. Our Si-air batteries exhibit a specific capacity of 269 Ah/kg and an average cell voltage of 0.85 V at a discharge current density of 7.9 µA cm^{-2}, corresponding to a specific energy of 229 Wh/kg.

Figure 1a shows the structure of the battery cell. In case of glass substrates, the electrical contact to the negative a-Si electrode on the left is provided by a thin conductive oxide (TCO) layer. In case of flexible stainless steel foils, the metal directly contacts the a-Si. A low concentration alkaline solution of potassium hydroxide (KOH) or sodium hydroxide (NaOH) serves as electrolyte. On the right of Figure 1a, a commercially available air electrode serves as positive electrode of the battery. The active layers of our Si-air batteries grow from plasma enhanced chemical vapor deposition at a deposition temperature T_{dep} = 170°C from silane SiH_4, methane CH_4 and phosphine (2 % PH_3 in SiH_4) as feedstock gases. A deposition rate of 10 nm min^{-1} yields 500 nm thick n-type a-Si and a-SiC layers. Figure 1b presents a photo of the a-Si electrode after full discharging, indicating that most of the a-Si is dissolved during discharge.

Figure 2 shows discharge curves of the a-Si and a-SiC anodes with different electrolytes, electrolyte concentrations and discharge currents. Table 1 gives detailed data for the discharge curves A through G. At present, the performance of these Si thin film batteries suffers from high self-discharge rates. Ongoing work will reduce the self-discharge and enhance specific capacity by using electrolytes like

EMI·2.3HF·F, room temperature ionic liquids (RTIL), and further improvement of the Si anodes. Thin film Si-air batteries easily integrate with flexible electronic devices or micro-electromechanical systems, and offer the potential of high specific capacity and energy density.

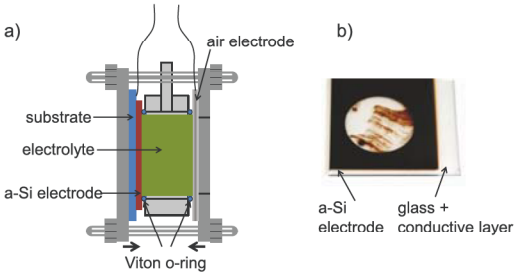

Figure 1:
a) Scheme of experimental silicon-air battery cell.
b) a-Si layer on conductive glass sub-strate of 2.7 cm diameter after full discharge.

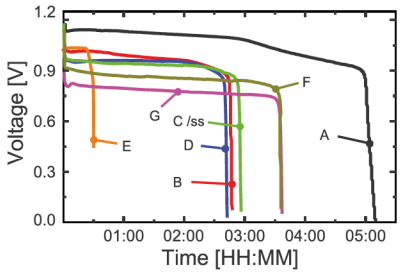

Figure 2:
Discharge curves of thin film Si-air batteries with anodes of a-Si (cells A to E) or-SiC (batteries F, G). The discharge current density j_d increases from A to E. Table 1 presents details on the variation of the alkaline electrolytes, electrode materials, and the resulting specific capacities.

Table I: Parameters and performance of thin film Si-air batteries at varying discharge current density j_d. The anodes of the batteries A, B, D-G are deposited on conducting Asahi-U, while battery C uses stainless steel (ss) as substrate and electrical contact.

Battery #	Anode material (n-type)	Source gas flow (sccm) $SiH_4/PH_3/CH_4$	Anode resistivity (Ω cm)	j_d (μA/cm)	Electrolyte, concentration (M)	Specific capacity (Ah/kg)
A	a-Si	3/3/0	440	1.6	KOH, 0.01	77
B	a-Si	3/3/0	440	7.9	KOH, 0.01	209
C /ss	a-Si	3/3/0	440	7.9	KOH, 0.01	219
D	a-Si	3/3/0	440	7.9	NaOH, 0.01	203
E	a-Si	3/3/0	440	31.4	KOH, 0.1	150
F	a-SiC	3/3/1	610	7.9	KOH, 0.01	269
G	a-SiC	3/3/3	3125	7.9	KOH, 0.01	262

Ablation of Silicon Nitride Layers with Pulsed ns Green Laser

Author: E. Hoffmann
In collaboration with: T. C. Röder, J. R. Köhler

This contribution presents the influence of silicon nitride ablation by a green pulsed ns laser on the ablation of silicon beneath the silicon nitride layer. After the irradiation with the laser intensity P_p = 7.5 × 10^7 W/cm^2, which is significantly below the known ablation threshold P_p = 2.9 × 10^8 W/cm^2 [1] of silicon, we observe ablated craters in the silicon surface. Numerical modelling of the temperature shows that sublimated SiN_x generates a gas pressure at the SiN_x/Si interface, which causes the ablation.

Figure 1 shows a schematic of the irradiation process. The silicon wafer is passivated by a silicon nitride layer, which is transparent to the incident laser radiation of wavelength λ = 532 nm. The silicon absorbs the laser radiation power I_p and heats. The thermal energy Q is conducted across the Si/SiN_x-interface by the heat flux q = λ dT/dz, where T is the temperature profile in vertical (z)-direction and λ the thermal conductivity of the materials. Due to the lower sublimation point of SiN_x compared to the boiling point $T_{B,Si}$ of silicon, the SiN_x decomposes into liquid silicon and nitrogen. Meanwhile, the silicon becomes liquid and turns into a superheated liquid, after exceeding its boiling point. The molecular nitrogen gas exerts an increasing pressure onto the remaining SiN_x layer until the layer tears.

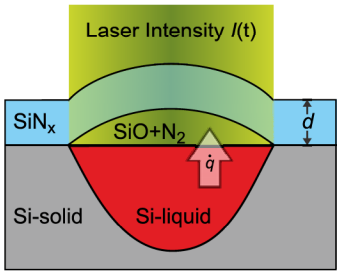

Figure 1:
Laser irradiation of a silicon nitride-passivated silicon wafer. Only the silicon absorbs the laser energy. The silicon nitride layer is heated by the heat flux $\dot{q}$ from the silicon. When the silicon nitride reaches its sublimation point, it decomposes into liquid silicon and nitrogen gas, which exerts a pressure onto the remaining layer.

During tearing, the high gas pressure squeezes out the liquid silicon melt, leaving a crater behind. We simulate the ablation process by numerically solving the two-dimensional heat transfer equation

$$c_P(T)\,\rho\,(T)\,\frac{\partial\,T(x,z,t)}{\partial\,t} = \nabla[\,\lambda\,(T)\nabla T(x,z,t)] + \alpha\,(T)I(x,z,t) \qquad (1)$$

with the specific heat capacity c_p, density $\rho(T)$ and absorption coefficient α. The gas pressure at the interface can be calculated from the temperature distribution in the SiN_x and defines the moment of ablation t_{abl}.

Figure 2 compares a) a measured crater depth profile with b) the temperature profile at the moment of ablation t_{abl}. The crater depths d_{abl} = 350 nm consist of the SiN_x thickness and the ablated silicon. The temperature profile shows the solid/liquid boundary at the silicon melting point $T_{M,Si}$ and the superheated liquid boundary at the silicon boiling point $T_{B,Si}$. At the moment of ablation, the depth of liquid/solid silicon boundary agrees with the measured crater depth.

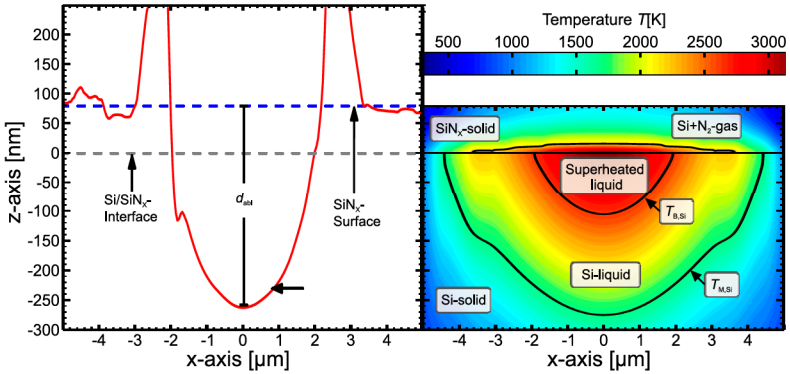

Figure 2:
a) Measured profile of an ablated crater in the silicon surface and b) calculated temperature profile at the moment of ablation t_{abl}. The measured ablation depth d_{abl} matches the depth of the liquid/ solid boundary in the silicon.

References:

[1] R. R. Karimzadeh, J. Zamir Anvari and N. Mansou, *Appl. Phys. A* **94**, 949 (2009).

Role of Phosphorus in Contact Formation on Silicon Solar Cells

Author: G. Kulushich
In collaboration with: R. Zapf-Gottwick

We reveal the role of phosphorus in contact formation between screen-printed silver paste and n-type emitter of industrial silicon solar cells. A higher inactive phosphorus (P) concentration at the emitter surface leads to a larger areal fraction of silver (Ag) crystallites at the contact. Thus, the specific contact resistivity is reduced. Inactive P atoms support the growth of Ag crystallites into the emitter by leaving the silicon lattice and forming an alloy of Ag/P within the Ag crystallites [1].

In order to investigate the contact between the silver paste and the emitter, the Ag bulk from the screen printed front contact and the glass layer under the Ag bulk formed during the co-firing process are etched off. The bare silicon surface shows the Ag crystallites also formed during firing. Scanning electron microscopy (SEM) and energy dispersive X-ray mapping (EDX) examine the contact area. Figures 1a-d illustrate that P is found at the positions of the Ag crystallites of the samples of emitter with high inactive P concentration.

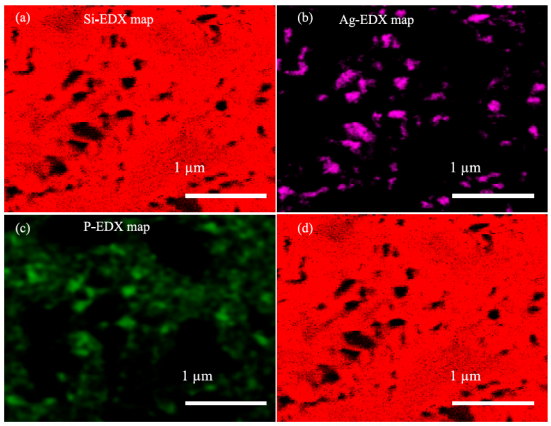

Figure 1:
Energy dispersive X-ray (EDX) mappings of the contact area of silver screen printed finger to emitter with high inactive phosphorous concentration $C_{in\text{-}P} \approx 10^{21}$ cm^{-3}. Detected elements are (a) silicon (Si), (b) silver (Ag), and (c) phosphorus (P); (d) EDX maps of Si, Ag, and P added together; P and Ag are detected at the same positions.

Due to the relatively low electron energy E = 5 keV, the detected X-ray signal comes from the shallow depths of the sample. Figure 1a depicts the EDX mapping of Si, showing black regions where Si is not detected, because the X-ray information depths end within the Ag crystallites. The intensity of the red color depends on the intensity of the detected X-ray signal at each pixel. The inhomogeneity in Fig. 1a is due to the pyramidal texture and due to remaining SiN_x not etched by the paste during firing. Figure 1b illustrates the EDX mapping of Ag; the regions without Ag are black, and the regions where Ag is detected are violet. Figure 1c shows the EDX of phosphorus. A higher green intensity at some areas indicates a higher P concentration. Figure 1d adds the EDX maps of Si, Ag, and P together and demonstrates that higher concentration of P is found at the positions of the Ag crystallites.

The inactive P from the emitter enhances the Ag crystallites growth into the Si-wafer during the firing process. During the firing process, phosphorus clusters probably sublimate and diffuse into the silver, leaving vacant places in the lattice. Silver uses the disturbed surface of the silicon lattice for its first nucleation. Additionally, it is possible that P from the SiP-precipitates leaves the SiP crystal and diffuses into Ag.

The results show that the *inactive* phosphorus in the emitter plays a crucial role in the contact formation. The inactive P atoms from the emitter help the silver crystallites to nucleate and to grow into the silicon lattice. Higher concentration of P is detected at the positions of the Ag crystallites compared to the neighboring emitter, pointing out that an Ag/P alloy is formed during the industrial firing process.

References:

[1] G. Kulushich, R. Zapf-Gottwick, V. X. Nguyen, and J. H. Werner, phys. stat. sol. RRL, **6**, 370 (2012) / DOI 10.1002/pssr.201206298

Rear Side Passivation for Crystalline Silicon Solar Cells

Author: K. Carstens
In collaboration with: M. Dahlinger, M. Schubert

We passivate industrial silicon solar cells with a-SiO_x:H deposited by plasma enhanced chemical vapor deposition at an industrially feasible low frequency f = 40 kHz. The surface recombination velocity on the rear side of the cells after a firing step in contact with aluminum paste is below $S_{fired,rear}$ = 30 cm/s. First PERC-type solar cells show an efficiency η = 18 % on 239 cm^2 active area.

After a fast firing step at a temperature T_{firing} = 800°C, the effective lifetime amounts τ_{aSiOx} 200 µs for all precursor gas flow ratios. After wafer cleaning, we deposit a-SiO_x:H on both sides in a PECVD system using a gas mixture of silane (SiH_4) and nitrous oxide (N_2O) with precursor gas flow ratios q = [N_2O]/([N_2O]+[SiH_4]). Figure 1 shows effective lifetimes τ_{eff} for different gas flow ratios q, as deposited as well as after single side aluminum screen printing and a fast firing step at 800 °C. A high as-deposited lifetime requires to precisely maintain the precursor gas flow ratio. After a fast firing step, the effective lifetime shows about τ_{aSiOx} = 200 µs for all samples. This value corresponds to a surface recombination velocity below $S_{fired,rear}$ = ½ $w \cdot (\tau_{asiox}^{-1} - \tau_b^{-1})$ = 30 cm/s, with a wafer thickness w = 170 µm and an assumed bulk lifetime τ_b = 500 µs. We choose a gas flow ratio q = 0.33 for the production of first solar cells.

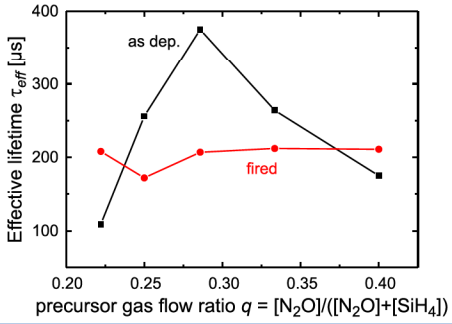

Figure 1:
The precursor gas ratio q is an important parameter to achieve a high as deposited effective lifetime τ_{eff}. The highest lifetime τ_{aSiOx} = 380 µs is achieved at a ratio q = 0.28.

Figure 2a explains the industrial type process we use to manufacture crystalline silicon solar cells from 239 cm^2 large monocrystalline Cz-wafers. It consists of i) texturing, ii) a phosphorus doped 65 Ohm/sq. emitter, iii) a PECVD silicon nitride antireflection and surface passivation layer on the front side, iv) a parasitic emitter removal etch in diluted potassium hydroxide (KOH), v) the a-SiO_x:H/SiN_x passivation layer stack, vi) laser ablation of 5 % to 10 % of the passivated area on the rear, followed by vii) a short KOH etching step, viii) screen printing of silver front contacts and aluminum rear contacts and finished by fast-firing.

Figure 2b shows the resulting cell structure with an a-SiO_x:H layer as rear side passivation. A cell produced with this process-sequence resulted in an efficiency η = 18 % with open circuit voltage V_{oc} = 624 mV, short circuit current density J_{sc} = 38 mA/cm^2 and a fill factor *FF* = 75.9 %.

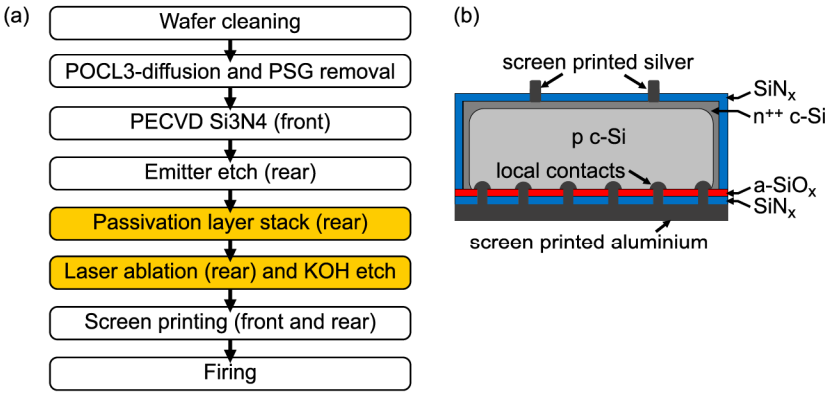

Figure 2:
a) Process sequence. The shaded steps show the additional steps compared to a standard solar cell. b) Schematic drawing of the finished solar cell with local contacts through an a-SiO_x/SiN_x passivation layer.

Stress in Silicon during Laser Irradiation

Author: K. Ohmer
In collaboration with: P. Lill, J. R. Köhler

The *ipv* developed a selective laser doping process, which increases the doping concentration and the depth of the emitter. Laser parameters, like the energy density and focus shape, have a high impact on the development of defects [1]. During laser irradiation silicon melts and recrystallizes epitaxially afterwards. Due to high temperature gradients, stress generates defects, if it exceeds a critical value. Using a line focus for irradiating a wafer with a (111)-surface, the tension along the long axis leads to the development of dislocations mostly having Burgers vectors lying in the (111)-plane [2].

We developed a C^{++} computer code, which numerically solves the heat transport equation

$$\frac{\partial T(x,z,t)}{\partial t} = \frac{1}{c_p(T)\rho(T)}\left[\nabla(\lambda_{th}(T)\nabla T(x,z,t)) + \alpha(T)I(x,z,t)\right] \qquad (1)$$

and the temperature dependent differential equations of the elastostatics

$$(2\mu+\lambda)\left[\frac{\partial^2 w}{\partial z^2} - \frac{\partial(\alpha_{th}\Delta T)}{\partial z}\right] + \lambda\left[\frac{\partial^2 u}{\partial x \partial z} - 2\frac{\partial(\alpha_{th}\Delta T)}{\partial z}\right] + \mu\left[\frac{\partial^2 w}{\partial x^2} + \frac{\partial^2 u}{\partial x \partial y}\right] = 0 \qquad (2)$$

$$(2\mu+\lambda)\left[\frac{\partial^2 u}{\partial x^2} - \frac{\partial(\alpha_{th}\Delta T)}{\partial x}\right] + \lambda\left[\frac{\partial^2 w}{\partial x \partial z} - 2\frac{\partial(\alpha_{th}\Delta T)}{\partial x}\right] + \mu\left[\frac{\partial^2 u}{\partial z^2} + \frac{\partial^2 w}{\partial x \partial z}\right] = 0 \qquad (3)$$

simultaneously. Due to the high aspect ratio of the line focused laser beam the equations can be solved in two dimensions *x*, and *z*, pointing in direction of the short axis of the laser focus and perpendicular to the wafer surface. Here *T* is the temperature, c_p the specific heat, ρ the density, λ_{th} the heat conductivity, α the absorption coefficient and *I* the time-dependent power density of the laser beam.

Local heating of the silicon leads to a volume expansion. The resulting displacement fields *u* and *w* are oriented along the short

axis of the laser focus (x-direction) and perpendicular to the wafer surface (z-direction). Here λ and μ are the Lamé parameters and α_{th} is the thermal expansion coefficient. Tensile and shear stresses depend on the displacement vector $\vec{s}$ = (*uvw*) according to

$$\sigma_{ij} = \lambda\left(\mathrm{Spur}\left(\underline{\varepsilon} - \alpha\Delta T \cdot \mathrm{I}\right)\right)\delta_{ij} + 2\mu\left(\varepsilon_{ij} - \frac{1}{3}\mathrm{Spur}\left(\alpha\Delta T \cdot \mathrm{I}\right)\delta_{ij}\right) \quad \text{with} \quad \varepsilon_{ij} = \frac{1}{2}\left(\partial_i s_j + \partial_j s_i\right).$$

Figure 1 shows the stress fields evolving in a silicon wafer irradiated with a 10 ns laser pulse of energy E_p = 0.5 mJ, a focus of width w = 20 nm and length l = 500 μm, shortly before the silicon starts to melt. Figures 1(a), 1(b) and 1(c) show tensile stresses parallel to the short and long axis σ_{xx}, σ_{yy} and perpendicular to the surface σ_{zz}. Figure 1(d) presents the shear stress in the xz-plane σ_{xz}. The maximal tensile stress develops along the short and the long axis, while σ_{zz} remains comparable small. In this direction, tension is reduced by the upward expanding wafer surface. Also the shear stress reaches values two orders in magnitude smaller.

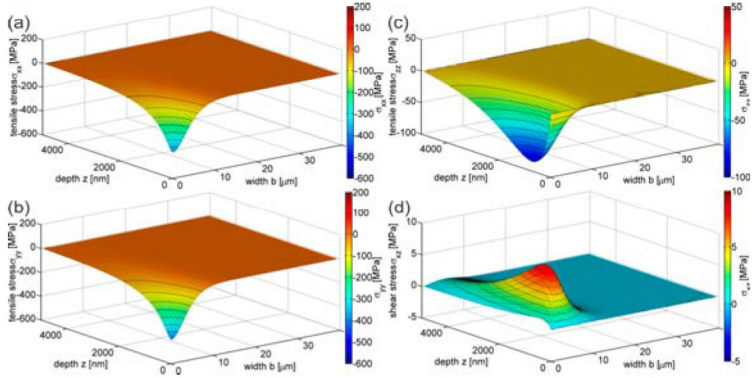

Figure 1:
Tensile stress σ_{xx}, σ_{yy}, σ_{zz} and shear stress σ_{xz} during laser irradiation.

References:

[1] K. Ohmer, Y. Weng, J. R. Köhler, H. P. Strunk, and J. H. Werner, IEEE J. Photovoltaics **1**, 183-186 (2011).

[2] Y. Weng, B.Kedjar, K. Ohmer, J. R. Köhler, H. P. Strunk, and J. H. Werner, phys. stat. sol. **C 1**, 28-31 (2013).

Limits in the Conductivity of Metallization Pastes

Author: L. Hamann
*In collaboration with: R. Zapf-Gottwick, J. Mattheis**

Reducing the amount of silver reduces the cost of solar cells. Usually, the silver consumption is lowered by the reduction of this metal in the contact paste. We present a new paste with silver coated nickel particles, reducing the silver amount without decreasing the metal content and still keeping the properties of silver related to oxidation and sintering. Coating pastes decrease the silver consumption for rear side bus bars to $c_{Ag} < 1.4$ mg/cm^2, leading to a conductivity $\sigma_{BB} = 1.1 \times 10^5$ S/cm, without decreasing cell or module efficiency. The conductivity of coating pastes is too low using coating pastes as a replacement for the metallization paste for grid fingers, but good enough to replace the silver paste for busbars with a cheap alternative [1].

To show the influence of the porosity of fired metallization pastes on the conductivity, we produce different pastes, containing either silver as metal or silver-coated nickel as metal particles. The Solsol GmbH mixes metallization pastes containing metal powder, an optimized glass frit composition and an organic binder combined with a solvent to reach good printability of the paste. To vary the porosity, we change the size of the particles and vary the belt speed of the firing furnace. Apart from the particle size, the paste formulation is kept constant to keep the pastes comparable. After firing, we measure the line resistance of the contact via 4-point measurement and the dimension of the fired paste via scanning electron microscope measurements to calculate the conductivity σ and the porosity *P*, taking the weight and dimensions into account. A Finite-Element-Method simulation calculates the influence of pores in the paste on the electrical conductivity σ. Figure 1a shows that the measured conductivity of silver (Ag) $\sigma_{meas,Ag}$ and silver coated nickel (AgNi) $\sigma_{meas,AgNi}$ pastes decrease with higher porosity *P*.

*(*Solsol GmbH)*

The simulated σ of Ag and AgNi paste show the same trend but the measured values are always smaller than the simulated ones. The comparison to evaporated Ag with P = 0 % shows with an annealing process at temperatures T = 160 °C that σ increases to the literature value which is the starting point at P = 0 % for the simulation. Supposing, that an oxidation layer between core metal and silver coating prevents the core contribution to the conductivity, we calculate the core metal as porous, non-conductive material. Figure 1b shows in addition to Fig.1a the recalculated P of $\sigma_{AgNi,meas}$ giving a shift in σ to $\sigma_{AgNi,meas,Ni\ isolated}$ which now fits very well to $\sigma_{meas,Ag}$. The results show that the Ni-core does not contribute to the conductivity of the paste after firing but the Ni-core is able to decrease the amount of Ag in the paste.

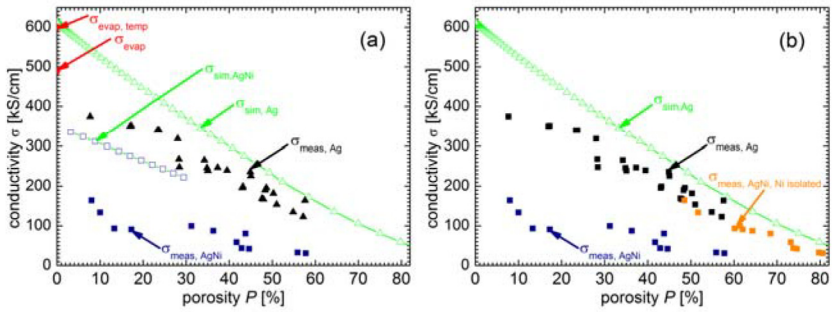

Figure 1:
a) Measured conductivity σ of silver (Ag) $\sigma_{meas,Ag}$ and silver coated nickel (AgNi) pastes $\sigma_{meas,AgNi}$ decrease with increasing porosity P. The simulated conductivity of Ag paste $\sigma_{sim,Ag}$ and of AgNi paste $\sigma_{sim,AgNi}$ show the same trend but with $\sigma_{AgNi,meas} < \sigma_{AgNi,sim} < \sigma_{Ag,sim}$. Evaporated Ag serves as a reference with porosity P = 0 %. The conductivity of the evaporated Ag $\sigma_{Ag,evap,meas}$ increases after tempering at T = 160 °C to the literature value $\sigma_{Ag,ev,temp}$. b) Recalculation of P where the core material Ni acts as non-conductive media, results in a shift of $\sigma_{AgNi,meas,Ni\ isolated}$ to higher porosities. $\sigma_{AgNi,meas,Ni\ isolated}$ fits well to the calculated $\sigma_{Ag,sim}$ indicating that the core material does not play a part in conductivity.

References:

[1] L. Hamann, G. Benstetter, A. Hofer, J. Mattheis, M. Haas, and R. Zapf-Gottwick, IEEE J. Photovolt. X, xxx (XXXX)

Thin Film Photo-Chips for Medical Applications

Author: M. Berner
In collaboration with: S. Vollmer, M. B. Schubert

Within the EU-project NANODEM (**NANO**photonic **DE**vice for **M**ultiple Therapeutic Drug Monitoring) the *ipv* develops highly sensitive amorphous silicon photodetectors for the visible range of radiation.

The project aims at the development of a Point-of-Care device for the monitoring of the free fraction concentration of immunosuppressive drugs in the blood of transplant patients [1]. Our detection method of the analyte concentration (the free fraction of the drug) bases on measurements of radiation emitted by excited, fluorescent markers in a microfluidic channel. In order to achieve the challenging detection limit for the drugs of interest, two different approaches are under development. One measures the fluorescent particles in the volume of the microfluidic channel – and therefore is called homogeneous approach. The other one detects the particles on one of the surfaces inside of the microfluidic channel – and therefore is called the heterogeneous approach. Both approaches use functionalized magnetic nanoparticles and strong planar electromagnets to perform the biochemical assay and to enhance the fluorescence signal.

The *ipv* develops the optical detector chips required by the two approaches. The different needs of the two approaches lead to completely different geometrical layouts of the optical detector chips and the thin film photodiodes on the chips. The homogeneous approach requires four photodiodes per channel with an active area A = 1 mm^2 each; the heterogeneous approach requires just one diode per channel, but with a large active area A = 36.3 mm^2. Figure 1 shows the uniform external quantum efficiency *EQE* for all three photodiodes of a preliminary (3-channel) optical detection chip for the heterogeneous approach fabricated at the *ipv*.

Apart from the freedom in tailoring the layout of the photodiodes, the use of hydrogenated amorphous silicon (a-Si:H) also allows for adjusting of their spectral responsivity (or *EQE*). Therefore, the a-Si:H improves the suppression of the excitation radiation for both approaches of the NANODEM project. A high sensitivity requires separating the fluorescent radiation and the radiation of the excitation. Furthermore, a-Si:H pin-photodiodes offer a very low dark current density level [2], which improves the signal-to-noise ratio *SNR* of the detectors. Such a low dark current level is particularly essential to achieve a high resolution for the fluorescence signal. Thus, the system reaches also a high sensitivity and resolution of the free fraction concentration of the immunosuppressive drug.

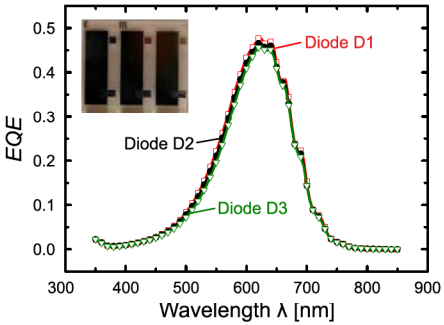

Figure 1:
External quantum efficiency *EQE* of all three pin-diodes of a 3-channel optical detector chip for the heterogeneous approach of the NANODEM project. The photodiodes have an active area A = 36.3 mm^2 each. Inset shows a photo of the chip.

References:

[1] http://nanodem.ifac.cnr.it/index.php/project-overview
[2] M. Sämann, D. Furin, J. Thielmann, A. Pfäfflin, G. Proll, C. Harendt, G. Gauglitz, E. Schleicher and M. B. Schubert, phys. stat. sol. **C 7**, 1160-1163 (2010).

Laser Doped Screen Printed Back Contact Solar Cells Exceeding 21 % Efficiency

Author: M. Dahlinger
In collaboration with: K. Carstens, J. R. Köhler, R. Zapf-Gottwick, and J. H. Werner

The *ipv* recently presented laser doped back contact solar cells metallized with evaporated and photo-lithographically structured contacts yielding an efficiency η = 22.0 % [1]. To make solar cell processing industrially relevant, we used Czochralski n-type wafers, laser ablation for local contact opening, applied a selective emitter doping, and utilized standard screen printed contacts. The best solar cell with a size of 2×2 cm^2 reaches an efficiency of η = 21.4 % [2].

For metallization we used an experimental silver based screen printing paste which contacts n-type as well as p-type doped silicon. Consequently only one screen printing step and one drying step is required. After screen printing, drying, and firing, we measured the contact resistance by the transfer length method. Fig. 1 shows the sheet resistance dependence of the contact resistance on n-type and p-type doped regions. The contact resistance ρ_c linearly increases with the sheet resistance R_{sh} for both n-type and p-type doping. The n-type back surface field (BSF) of our solar cells is heavily doped resulting in a sheet resistance of $R_{sh,BSF}$ = 12 Ω/sq. The corresponding contact resistance is $\rho_{c,BSF}$ < 0.5 mΩcm^2. Although the contact resistance to the p-type emitter is lower for a certain sheet resistance a reasonable emitter saturation current requires a sheet resistance $R_{sh,HE}$ > 60 Ω/sq. For $R_{sh,HE}$ ≈ 115 Ω/sq, the contact resistance is $\rho_{c,HE}$ ≈ 4.0 mΩcm^2, which limits the fill factor. A selective emitter doping with a sheet resistance $R_{sh,SE}$ ≈ 45 Ω/sq under the contacts reduces the contact resistance to $\rho_{c,SE}$ ≈ 1.4 mΩcm^2 and decreases the series resistance significantly.

Table 1 shows the averaged results of current density/voltage J/V-measurements of cells with and without selective emitter. The selective emitter increases the mean open circuit voltage V_{oc} by ΔV_{oc} = 3 mV. The low front surface recombination combined with low front side re-

flection and good light trapping on 8 Ωcm bulk material enable a short circuit current density $J_{sc} \approx 42$ mA/cm^2. The mean *FF* increases by $\Delta FF = 2.7$ %, due to the reduced contact resistance. The mean efficiency increases by $\Delta\eta \approx 0.9$ %$_{abs}$ to $\eta \approx 21.2$ % with selective emitter doping. The best solar cell achieves an efficiency $\eta \approx 21.4$ %.

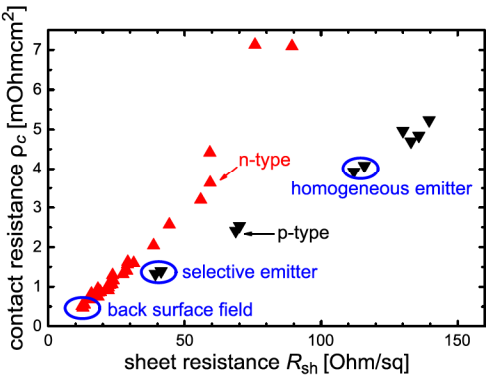

Figure 1:
Contact resistances achieved with screen printing the same paste on laser doped n-type and p-type sur-faces.

Table I: Open circuit voltage V_{oc}, short circuit current density J_{sc}, fill factor *FF*, and efficiency η of cells each with and without selective emitter doping (mean of 3 cells).

	V_{oc} [mV]	J_{sc} [mV/cm^2]	*FF* [%]	[%]
with SE	654	42.0 ±0.1	77.3 ±0.9	21.2 ±0.2
without	651 ±1	41.8 ±0.1	74.6 ±0.8	20.3 ±0.2

References:

[1] M. Dahlinger, B. Bazer-Bachi, T. C. Röder, R. Zapf-Gottwick, J. R. Köhler, and J. H. Werner *Energy Procedia* **38**, 250 (2013).

[2] M. Dahlinger, K. Carstens, R. Zapf-Gottwick, J. R. Köhler, and J. H. Werner *Energy Procedia* **55**, 410 (2014).

Worst Case Leaching of PV modules

Author: R. Zapf-Gottwick
In cooperation with: F. Schwerdt, L. Hamann, J. H. Werner, M. Koch, K. Fischer*, M. Kranert*, J. W. Metzger**

Photovoltaic modules contain hazardous substances. On the one hand, even if the solar cells themselves are free of toxic elements or compounds (as is the case of modules from either crystalline, microcrystalline or amorphous silicon) the soldered ribbons within the modules contain the toxic heavy metal lead (Pb). The same holds also for the thin film modules from cadmium sulfide/cadmium telluride CdS/CdTe and copper indium gallium diselenide Cu(In,Ga)Se_2 (CIGS). On the other hand, in case of such CdS/CdTe modules, the semiconductors themselves making up the heterojunction cells are toxic. In case of CIGS modules, the compound Cu(In,Ga)Se_2 seems less toxic, however, most manufacturers of such modules use the toxic CdS as part of the window layer.

This study investigates leaching of hazardous substances out of photovoltaic modules containing crystalline silicon solar cells (c-Si), CdTe, CIGS, or amorphous silicon (a-Si). In our worst case study, milled module pieces release a high amount of lead and cadmium into the water based solution with a strong dependence on the pH value. With three different solutions, we simulate different environmental conditions: i) “low mineralized water” conditions, via water containing sodium hydroxide, ii) “sea water” conditions, via water containing sodium hydroxide and sodium chloride, and iii) “rainwater” conditions, via water containing acetic acid. Figure 1 shows that in “rain water”-like solutions with low pH values, already after a few days, more than 50 % of the Cd is leached out from milled CdTe module pieces! Tellurium elutes in the range of 40 % without dependence on the pH value of the solution, indicating an instable CdTe-bonding. In the same time, more than 15 % of lead is leached out from c-Si module pieces. Table I shows the corresponding studies on CdTe and c-Si modules which fit very well to our measured data without dependence on the size of the eluted module pieces.

*(*ISWA, Institut für Siedlungswasserbau, Wassergüte- und Abfallwirtschaft)*

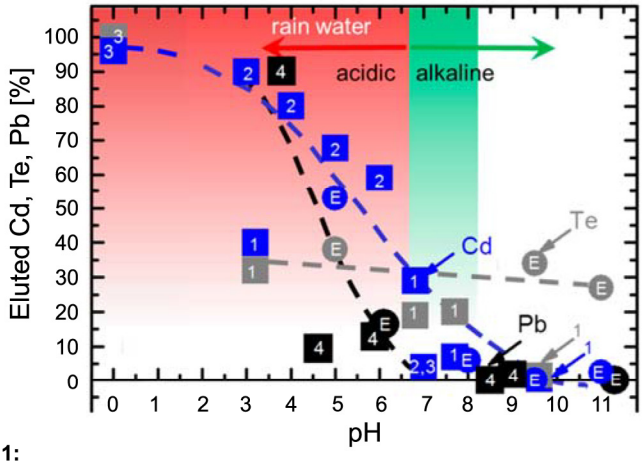

Figure 1:
Eluted cadmium (Cd), tellurium (Te), and lead (Pb) in solutions with different pH. Different colors correspond to different elements. Our own experiments are marked with an "E"; we give the pH at the end of our experiments. Data, marked with numbers from 1 to 4, stem from literature (see first column of Table I.) Dashed lines are guide-lines to the eye showing that our data fit to the literature data. Leaching of Cd and Pb highly depends on the pH. In particular, in the acidic range (regime of "landfill" and "rain water") both toxic metals are heavily leached out. In contrast, Te leaching depends only weakly on pH.

Table I: Previous leaching studies on CdTe- and c-Si-modules. The size of module pieces, leaching time and pH of the leaching solution is given; eluted elements and corresponding pH are plotted in figure 1.

No.	Reference	Module	Size
1	G. Okkenhaug, Norwegian Geotechnical Institute, NGI report No. 20092155-00-1-R (2010)	CdTe	125 µm < 4 mm
2	J. Allen, Z. Kiss, S. Annamalai, I. L. Pegg, B. Dutta, 2010, private communication	CdTe	5x5 cm^2
3	V. M. Fthenakis, W. Wang, Prog. Photovolt. Res. Appl. 14, 363-371 (2006)	CdTe	< 1 cm^2
4	H. P. Arp, G. Okkenhaug, M. Sparrevik, Norwegian Geotechnical Institute, NGI report No.20100446-00-2-R (2010)	c-Si	125 µm < 4 mm

Mismatch Loss in Photovoltaic Systems

Author: *T. S. Wurster*
In collaboration with: M. B. Schubert

Current mismatch and shading effects on the output of single photovoltaic (PV) modules are well analyzed, but only few reports address mismatch losses at a PV system level. For example, what happens if m PV strings with different numbers n of modules are connected in parallel? In such a case, the system builder must decide whether to use inverters with multiple maximum power point (MPP) trackers, module-power optimizers, or to shorten all strings for balancing the system. Our findings [1], calculated with the well known one-diode model (ODM), open new options. Numerical modeling of strings of different length in parallel to several others having an equal module count n renders mismatch losses below 1 % for most configurations: Where one string is one module shorter than the others, mismatch losses L range at $L < 0.5$ %. Therefore, strings of different length may favorably be connected to a cost-effective single-MPP inverter without significant energy yield losses. Also, thin film modules are less sensitive to mismatch than crystalline silicon modules.

Figure 1 presents the mismatch analyses. In order to assess the necessity or benefit of a string level MPPT, the simulated configurations incorporate m-1 identical strings of n+1 modules length, all parallel connected to one string with n modules. The simulation covers n = 10 to 20 modules per string, and m = 2 to 40 strings connected in parallel. Each line in Fig. 1 represents the series connection of a distinct number of n PV modules in the long strings, e.g. the top data set contains n+1 = 11 PV modules in the long strings, and n = 10 modules in the additional shorter string. The lines unite simulated configurations with a certain length n of their short string. The relative mismatch loss L decreases for $m > 3$ strings connected in parallel, independent of n. For all string lengths $n \geq 10$, configurations with $L_{ODM} < 1$ % exist, but $n \geq 11$ is necessary to obtain $L_{ODM} < 0.5$ %.

These findings underline that most systems are robust by design, questioning the necessity of expensive multiple-MPPT inverters or power optimizers. However, a system 'mismatched by design' is more prone to additional mismatch losses by shading. On the other hand, less electronic components imply less risk of failure, thus encouraging the most simple system design that provides similar annual energy yield.

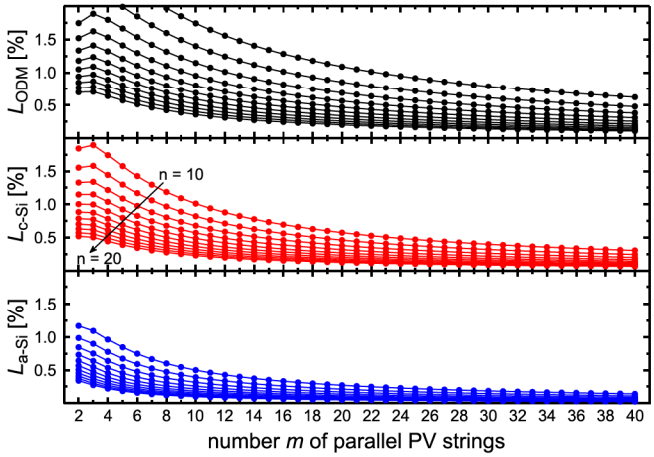

Figure 1:
Calculated loss *L* for PV systems with m parallel strings, each with n modules. The One Diode Model (ODM), most sensitive to mismatch, shows the highest losses, followed by the c-Si configurations. The a-Si configurations are less prone to mismatch losses.

References:

[1] T. S. Wurster and M. B. Schubert, Solar Energy **105**, 505 (2014).

Pulsed Laser Transfer of Nickel Thin Films on Glass

Author: T. C. Röder
In collaboration with: J. R. Köhler

Our pulsed laser transfer process transfers thin nickel layers from a glass substrate onto silicon wafers. Applications are the front- and back-side metallization of solar cells. The metallization process achieves thin front side fingers of width $w < 30$ µm [1] resulting in less metal covered area compared to standard screen printed contacts. We use a pulsed green laser to transfer nickel from a glass substrate and directly contact the emitter of solar cells through the anti-reflection coating.

We developed a numerical simulation model, which solves the heat transport equation in the glass and nickel layer. The numerical simulation models the phase transitions for melting and evaporation of both glass and nickel as well as the absorption of the laser radiation in both layers. The transfer process is modelled by calculating the vapor pressure P resulting from the evaporated material. Our numerical calculations identify two possible transfer mechanisms: the transfer of completely molten layers and partly molten layers. Which of these two transfer process takes place, strongly depends on the thickness of the nickel layer and on the duration of the laser pulse.

Figure 1 explains the two transfer mechanisms. For completely molten nickel layers, the gas pressure creates a liquid nickel bubble. The nickel bubble bursts if the vapor pressure inside the bubble reaches its critical value, which mainly depends on the surface tension of liquid nickel. For thick nickel layers, the transfer process occurs before the nickel layer is completely molten. The vapor pressure expands the solid part of the nickel layer, until the resulting tensile stress reaches the critical value for solid nickel and the layer bursts.

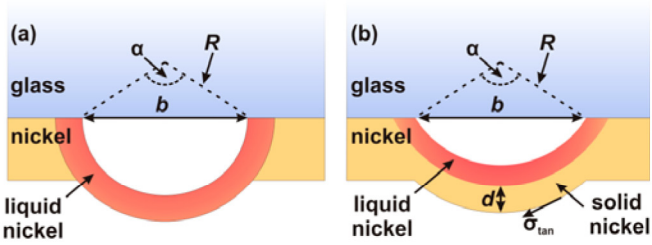

Figure 1:
Scheme of laser transfer mechanisms for (a) completely molten and (b) partly molten nickel layers.

Figure 2 shows the influence of the laser pulse duration on the temperature profile inside the nickel layer at the moment, when the transfer process takes place. In this example the nickel layer has a thickness d = 220 nm. Here, only laser pulses with a duration $\tau \geq 8$ ns, lead to the transfer of completely molten nickel.

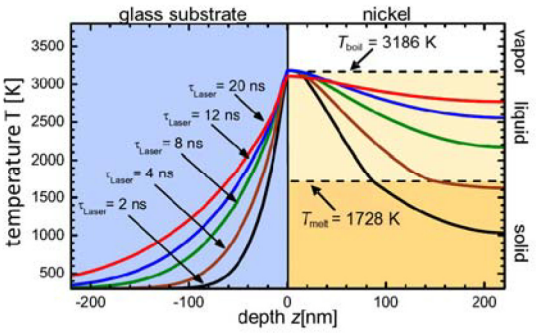

Figure 2:
Influence of the laser pulse duration t_{FWHM} on the temperature profile in the glass substrate and a d = 220 nm thick nickel layer at the moment, when the transfer process takes place.

References:

[1] T. Röder, E. Hoffmann, J. R. Köhler, and J. H. Werner, in *Proc. 35th IEEE Photov. Spec. Conf.* (IEEE, Piscataway, NY, 2010), p. 3597.

Publikationen
Publications

Rear Side Passivation for Crystalline Silicon Solar Cells
K. Carstens, M. Dahlinger, and M. B. Schubert, in *Proc. of the 2nd International Education Forum on Environment and Energy Science*, (Tokyo Institute of Technology, Tokyo 2013), DOI: 10.13140/2.1.3044.3841

Industrial Implementation of Metal Assisted Texture for Multi-crystalline Silicon Solar Cells
J. Cichoszewski, M. Reuter, V. Speer, G. Willers, H. J. Axmann, and J. H. Werner, in *Proc. 22nd International Photovoltaic Science and Engineering Conference* (2012), DOI: 10.13140/2.1.4058.6563

Role of Catalyst Concentration on Metal Assisted Chemical Etching of Silicon
J. Cichoszewski, M. Reuter, F. Schwerdt, and J. H. Werner, Electrochem. Acta **109**, 333 (2013)

22.0 % Efficient Laser Doped Back Contact Solar Cells
M. Dahlinger, B. Bazer-Bachi, T. Röder, J. R. Köhler, R. Zapf-Gottwick, and J. H. Werner, Energy Procedia **38**, 250-253 (2013), DOI: 10.1016/j.egypro.2013.07.274

Laser Doped Screen-printed Back Contact Solar Cells Exceeding 21 % Efficiency
M. Dahlinger, K. Carstens, J. R. Köhler, R. Zapf-Gottwick and J. H. Werner, Energy Procedia **55**, 410-415 (2014), DOI: 10.1016/j.egypro.2014.08.118

Laserdotieren von Siliziumsolarzellen
S. Eisele, Verlag Dr. Hut, München, Deutschland,
ISBN 978-3-8439-0312-7, (2012)

In-situ Series Connection of Amorphous Silicon Tandem Module
A. Garamoun, R. Merz, S. Miyajima, and M. B. Schubert, physica status solidi (RRL) - Rapid Research Letters, 963 (2013), DOI: 10.1002/pssr.201308016

Thin-Film Silicon for Flexible Metal–Air Batteries
A. Garamoun, M. B. Schubert and J. H. Werner, ChemSusChem, **7**, 3272–3274 (2014), DOI: 10.1002/cssc.201402463

Colored Ribbons Achieve +0.3 % abs Module Efficiency Gain
L. Hamann, L. Proenneke, M. Reuter, and J. H. Werner, in *Proc. 22nd International Photovoltaic Science and Engineering Conference* (2012), DOI: 10.13140/2.1.5107.2327

Replacing Silver by Base Metal Saves 30 % Silver Costs on Bus Bars
L. Hamann, M. Haas, J. Mattheis, and R. Zapf-Gottwick, in *Proc. of the 2nd International Education Forum on Environment and Energy Science*, (Tokyo Institute of Technology, Tokyo 2013), DOI: 10.13140/2.1.2798.6249

30% Silver Reduction in Rear Bus Bar Metal Paste
L. Hamann, M. Haas, W. Wille, J. Mattheis, and R. Zapf-Gottwick, Energy Procedia **43**, 72-79 (2013)

Effect of Silicon Dioxide Ablation During Laser Transferred Contacts Process
E. Hoffmann, T. Roeder, J. R. Köhler, and J. H. Werner, in *Proc. of the 2nd International Education Forum on Environment and Energy Science*, (Tokyo Institute of Technology, Tokyo 2013), DOI: 10.13140/2.1.2150.5608

Origin and Spectral Degradation of the Photoluminescence from a-SiO_x
J. Kistner and M. B. Schubert, J. Appl. Phys. **114**, 193505 (2013), DOI: 10.1063/1.4829285

Impact of the Hydrogen Content on the Photoluminescence Efficiency of Amorphous Silicon Alloys
J. Kistner and M. B. Schubert, J. Appl. Phys. **114**, 213515 (2013), DOI: 10.1063/1.4841015

Metallization Losses in Industrial Silicon Solar Cells
G. Kulushich, http://www.dr.hut-verlag.de/9783843918787.html (2014)

Seasonal Performance Comparison of Different Photovoltaic Technologies Installed in Cyprus and Germany
G. Makrides, B. Zinsser, M. Schubert, G. E. Georghiou, International Journal of Sustainable Energy **32,** 466 (2013), DOI: 10.1080/14786451.2012.759572

Performance Loss Rate of Twelve Photovoltaic Technologies under Field Conditions Using Statistical Techniques
G. Makrides, B. Zinsser, M. Schubert, G. E. Georghiou, Solar Energy **103**, 28 (2014), DOI: 10.1016/j.solener.2014.02.011

Analysis of Photovoltaic System Performance Time Series: Seasonality and Performance Loss
A. Phinikarides, G. Makrides, B. Zinsser, M. Schubert, G. E. Georghiou, Renewable Energy **77**, 51 (2015), DOI: 10.1016/j.renene.2014.11.091

Fluorescent Materials for Silicon Solar Cells
L. Prönneke,
http://elib.uni-stuttgart.de/opus/volltexte/2012/7677/pdf/Proenneke_genehmigteAbhandlung.pdf, (2012)

Photocurrent Collection Efficiency Mapping of a Silicon Solar Cell by a Differential Luminescence Imaging Technique
U. Rau, V. Huhn, L. Stoicescu, M. Schneemann, Y. Augarten, A. Gerber, B.E. Pieters, Appl. Phys. Lett. **105,** 163507 (2014), DOI: 10.1063/1.4898008.

Lasermetallisierung für Siliziumsolarzellen
T. Röder, Verlag Dr. Hut, München, Deutschland, ISBN 978-3-8439-0820-7, (2012)

Light Trapping in Pyramidally Textured Crystalline Silicon Solar Cells Using Back-side Diffractive Gratings
R. Rothemund, T. Umundum, G. Meinhardt, K. Hingerl, T. Fromherz, and W. Jantsch, Prog. Photovolt: Res. Appl. **21**, 747 (2013), DOI: 10.1002/Pip.2192

Optical Modelling of the External Quantum Efficiency of Solar Cells with Luminescent Down-shifting Layers
R. Rothemund, Solar Energy Materials and Solar Cells **120**, 616 (2014), DOI: 10.1016/j.solmat.2013.10.004

Optimierung des Lichteinfangs von mikromorphen und einkristallinen Siliziumsolarzellen
M. Sämann, Verlag Dr. Hut, München, Deutschland, ISBN 978-3-8439-0585-7, (2012)

DaySy: Modulprüfung mittels Tageslicht-Lumineszenz
L. Stoicescu, M. Berner, M. Reuter, J. H. Werner, in *Proc. 29. Symposium Photovoltaische Solarenergie*, Bad Staffelstein, Germany (2014)

DaySy: Luminescence Imaging of PV Modules in Daylight
L. Stoicescu, M. Reuter, J. H. Werner, in *Proc. 29th Europ. Photovolt. Solar En. Conf.*, (WIP, München, 2014), p. 2553

Potential Variations Around Grain Boundaries in Impurity-Doped $BaSi_2$ Epitaxial Films Evaluated by Kelvin Probe Force Microscopy
D. Tsukahara, M. Baba, S. Honda, Y. Imai, K.O. Hara, N. Usami, K. Toko, J. H. Werner, T. Suemasu, J. Appl. Phys. **116,** 123709 (2014), DOI: 10.1063/1.4896760

Dislocation Formation During Laser Processing of Silicon Solar Cell Materials
Y. Weng, B. Kedjar, K. Ohmer, J. R. Köhler, H. P. Strunk, and J. H. Werner, Phys. Status Solidi C **10**, 28 (2013), DOI: 10.1002/pssc.201200548

Mismatch Loss in Photovoltaic System below 0.5 %
T. S. Wurster and M. B. Schubert, in *Proc. of the 2nd International Education Forum on Environment and Energy Science*, (Tokyo Institute of Technology, Tokyo 2013)

Mismatch Loss in Photovoltaic Systems
T. S. Wurster and M. B. Schubert, Solar Energy **105**, 505 (2014), DOI: 10.1016/j.solener.2014.04.014

Anpassungsverluste in Photovoltaiksystemen unter ein Prozent
T. S. Wurster and M. B. Schubert, presented at: *29. PV-Symposium*, Bad Staffelstein, Germany, (2014)

Lehrveranstaltungen
Lectures

Promotionen
Ph. D. Theses

Bachelorarbeiten
Bachelor Theses

Masterarbeiten
Master Theses

Gäste & ausländische Stipendiaten
Guests

Bauelemente der Mikroelektronik (Bachelor, 1. Semester)
J. H. Werner

Energiebänder und Leitfähigkeit
Silizium - der Werkstoff der Mikroelektronik
Elektronen und Löcher in Halbleitern
Ströme in Halbleitern
Nichtgleichgewicht und Injektion
Elektrostatik des pn-Übergangs
Ströme im pn-Übergang

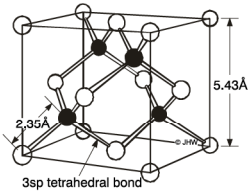

Energiewandlung (Master, 2. / 4. Semester)
J. H. Werner

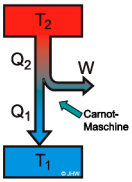

Grundlagen der Kernenergie
Thermodynamik
Direkte Nutzung der Sonnenenergie (Solarthermie, Photovoltaik)
Indirekte Nutzung der Sonnenenergie (Wasserkraft, Windenergie)
Chemische Wandlung und Speicherung elektrischer Energie

Laser and Light Sources (Master, 2. / 4. Semester)
J. H. Werner and J. R. Köhler

The Human Eye
Light and Color
Photometry
Incoherent Light Sources
Light Emitting Diodes
Lasers
Laser Processing

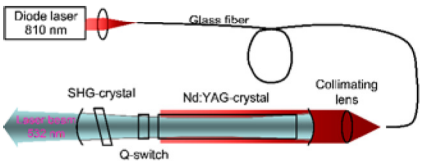

Optoelectronic Devices and Circuits I (Bachelor, 6. Semester)
J. H. Werner

Basic physics
Thermal radiation
Coherence
Semiconductor basics
Excitation and recombination processes in semiconductors
Light emitting diodes
Semiconductor lasers
Glass fibers
Photodetectors

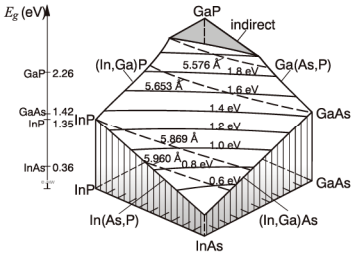

Photovoltaik I (Bachelor, 4. Semester)
J. H. Werner

Der Photovoltaische Effekt: Solarzelle, Solarmodul, Solaranlage
Sonnenspektrum und Energieverbrauch in Deutschland
Maximaler Wirkungsgrad einer Solarzelle
Grundprinzip einer Solarzelle
Ersatzschaltbilder
Photovoltaik-Materialien und -Technologien
Modultechnik
Photovoltaische Systemtechnik

Photovoltaik II (Master, 2. / 4. Semester)
J. H. Werner

Solarstrahlung
Alternativen zu konventionellen Siliziumzellen
Komponenten von Photovoltaikanlagen
Planung, Installation, Betrieb und Monitoring von Photovoltaikanlagen
Photovoltaische Messtechnik
Markt und Wirtschaftlichkeit der Photovoltaik

Photovoltaik III (Master, 1. / 3. Semester)
J. H. Werner

Technologie einkristalliner Zellen
Rekombinationsmechanismen
Theorie der maximalen Wirkungsgrade
Optimierungsstrategien
Zweite und Dritte Generation Photovoltaik

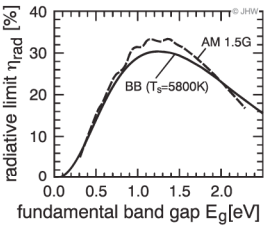

Wissenschaftliches Vortragen und Schreiben I (Wintersemester)
J. H. Werner

Kernbotschaften
Aufbau eines Vortrags
Standardfehler (Strukturfehler, Technikfehler, Fehler im Auftreten)
Praktische Schritte zum Vortrag
Selbst- und Fremdbeurteilung (mit Videoaufzeichung)

Wissenschaftliches Vortragen und Schreiben II (Sommersemester)
J. H. Werner

Kernbotschaften
Aufbau und Elemente einer Publikation
Bilder, Tabellen, Gleichungen und Referenzen
Verfassen eines eigenen wissenschaftlichen Kurzberichts
von 4 bis 6 Seiten

Praktische Übungen im Labor „Halbleitermesstechnik“ (Master)
R. Zapf-Gottwick und J. R. Köhler

Herstellverfahren von Halbleitern und dünnen Schichten
Elektrische Messtechniken für Minoritäten und Majoritäten
Optische Messtechnik
Strukturelle Messtechniken

Praktische Übungen im Labor „Photovoltaik“ (Bachelor)
R. Zapf-Gottwick und J. R. Köhler

Herstellung von industriellen kristallinen Si-Solarzellen
Messung und Auswertung der IV-Kennlinie
Quanteneffizienz und Reflexionsmessung
PV-Modulherstellung mit kristallinen Si-Solarzellen

Teamarbeit *ipv* (Bachelor)
R. Zapf-Gottwick und J. R. Köhler

Laminieren eines kristallinen Minimoduls
Löten eines Solarladereglers mit MPP-Tracking
Microcontrollerprogrammierung des MPP-Trackers

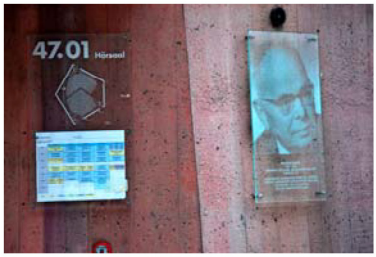

Promotionen
Ph. D. Theses

Gordana Kulushich
Metallization Losses in Industrial Silicon Solar Cells

Jens Kistner
Photolumineszenz von Silizium und Siliziumverbindungen

Gordana Kulushich

Jens Kistner

Bachelorarbeiten 2013 / 2014
Bachelor Theses 2013 / 2014

Felicia Bareis
Untersuchung der rückseitigen Kantenisolation an monokristallinen Solarzellen

Lukas Eber
Gesputterte Antimonschichten für laserdotierte Solarzellen

Anja Heinzelmann
Sinterprozess von Metallisierungspasten

Jonathan Höschele
Metallisierung von Rückseitenkontakt-Solarzellen

Sascha Koch
Dunkelkennlinienmessung an pin-Photodioden aus amorphem Silizium

Christoph Kohler
Lichtstreuung mittels Laserstrukturierung von EVA-Folie in cSi-PV-Modulen

Max Landeck
Filter zur Berechnung von Strahlungsspektren aus Dämpfungsmessungen

Lukas Lindel
Passivierung von Bor-Emittern mit amorphem Silizium

Hrvoje Marjanović
Ortsaufgelöster Stromtransportfaktor von Solarzellen

Tim Pfüller
Laserdotieren von n-Typ Solarzellen

Daniel Schaaf
Optimierung vergrabener Siebdruckkontakte

Niklas Straub
Entwurf eines Transformatorkonzepts für den Inselbetrieb von Energiespeichern

Daniel Wolpert
Photovoltaik-Carport für induktives Laden zweier Smart fortwo electric drive

Arno Wothe
Lotpasten für die Modulverschaltung von IBC-Solarzellen

Lea Zeiner
Feinlinienmetallisierung über Siebdruck

Master– und Forschungsarbeiten 2013 / 2014
Master and Research Theses 2013 / 2014

Hendrik Adler
Langzeitüberwachung von Photovoltaik-Anlagen

Rebekka Adler
Potentiale erneuerbarer Energien für einen philippinischen Schreinereibetrieb

Markus Botey-Junca
Aufbau eines Schlierenaufnahmeplatzes zur Untersuchung von Ablationsplasmen bei der Lasermaterialbearbeitung

Xiran Chen
Quantitatives Sintermodell von Metallpasten auf Solarzellen

Philipp Donn
Admittanzspektroskopie an Solarzellen

Kailas Bhaskar Gijare
Sensitivity Evaluation of An Extended PC1D-SPICE Two-Dimensional Solar Cell Simulator

Felix Hantsch
Plasmaunterstützte Gasphasenabscheidung von Al_2O_3 Passivierschichten

Simon Huber
Selbstjustierender selektiver Emitter

Jian Jin
Self-Adjusted Selective Emitter

Sascha Koch
Impedanzmessschaltung für Lithium-Ionen Akkus

Timo Kropp
Entwicklung eines Prototypen zur Arbeitspunktmodulation an Solarmodulen für Elektro- und Photolumineszenzaufnahmen

Simeon Kühl
Chemische Stabilität von EVA-Folie und mit EVA-Folie einlaminierten Schichten

Felix Kurz
Kamerabasierte Verschattungsanalyse und Prognose

Wanxin Ma
Implementierung eines Softwaresimulators für die Simulation von Radarmessungen

Kun Mo
Feinliniensiebdruck auf selektivem Emitter

Julian Oberacker
Design und Entwicklung eines hochempfindlichen Photostrommess-Systems

Niti Bharatkumar Panchal
Degradation Rate of Photovoltaic Systems

Georgios Psachoulias
Kontaktbildung während des Sintervorgangs

Salvador E. Martinez Regil
Modular CAN Controlled Power Switching System
Design and Implementation

Leander Rust
Heterojunction Solar Cell Analysis With Impedance Spectroscopy

Christian Sämann
Laserbehandeltes Dünnschichtsilizium als poröse
Anode in Lithium-Ionen-Batterien

Dengxia Wang
Langzeitdegradation von Photovoltaikmodulen

Florian Widmaier
Untersuchung und Bewertung des Daylight Lumineszenz System
in Hinblick auf die CE-Kennzeichnung

Andreas Zeuner
Einflüsse der Laserparameter auf die Laserkantenisolation

Gäste & ausländische Stipendiaten
Guests

Pedro Alpuim
Universidade do Minho, Guimarães, Portugal

Seyed Ali Mohammad Badri
Dalarna University, Falun, Schweden

Keelan Burns
Flinders University, Adelaide, Australien

Alex Fernando Borges Costa
Universidade Federal de São Carlos, São Carlos, Brasilien

Ebrahim Jamshidi Gohari
Dalarna University, Falun, Schweden

Maibi Malape
University of Fort Hare, Alice, Südafrika

Shinsuke Miyajima
Tokyo Institute of Technology, Tokyo, Japan

Jomar Julio Ruas
Pontifícia Universidade Católica de Minas Gerais, Brasilien

Satoshi Saijo
Nara Institute of Science and Technology, Nara, Japan

Aref Samadi
University of Teheran, Teheran, Iran

Kousaku Shimizu
CIT Nihon University, Narashino Chiba, Japan

Yue-Shun Su
National Tsing Hua University, Hsinchu, Taiwan

Was sonst noch war ...
More than Science ...

Mitarbeiterliste
Staff Members

Lageplan
Location Map

Was sonst noch war ...
More than Science ...

Tag der Wissenschaft

Am 22. Juni 2013 und am 12. Juli 2014 präsentierte sich das *ipv* wieder der interessierten Öffentlichkeit mit Informationen zu Photovoltaikmodulen und -anlagen. Im Rahmen von Führungen erklärten wir interessierten Gruppen die unterschiedlichen Solarzellentechnologien am Beispiel verschiedener Photovoltaikanlagen auf dem Dach des Gebäudes der Elektrotechnischen Institute.

Vortrag „Physik, die Wissen schafft"

Im Rahmen der vom Fachbereich Physik veranstalteten öffentlichen Vortragsreihe „Physik, die Wissen schafft" hielt Jürgen H. Werner am 7. Juli 2014 einen Vortrag mit dem Titel „Status und Zukunft der Photovoltaik", in dem er die Entwicklung der Photovoltaik in den letzten 20 Jahren umriss und aufzeigte, in welche Richtung die Weiterentwicklung der Photovoltaik gehen könnte.

Science Day

The *ipv* presented itself once more to the interested public on June 22nd in 2013 and July 12th in 2014. We showcased information on solar panels and solar plants. Guided tours to various photovoltaic installations on the roof of the building explained the different solar cell technologies to interested visitors.

Lecture "Physik, die Wissen schafft"

On July 7th 2014 Jürgen H. Werner presented the "Status And Future of Photovoltaics" within the series of public lectures "Physik, die Wissen schafft" (Physics Enlightens) arranged by the Department of Physics. He outlined the development of the photovoltaic technology during the past 20 years and explained in which direction the further development of this technology could go.


VORWE
RWE Z
IMPULS
VORWE
ipv

RWE Zukunftspreis

Dr. Sebastian Eisele vom Institut für Photovoltaik (*ipv*) der Universität Stuttgart hat für seine Doktorarbeit über das Laserdotieren von Siliziumsolarzellen den Zukunftspreis 2013 der RWE AG erhalten. 2013 wurden Arbeiten im Bereich Erneuerbare Energien prämiert. Hier zeichnete sich die Dissertation von Sebastian Eisele mit grundlegenden Arbeiten zu Laserprozessen für die Photovoltaik aus. Uwe Tigges, Mitglied des Vorstands der RWE AG, überreichte Dr. Sebastian Eisele für seine überragenden Leistungen den mit 13.000 € dotierten ersten Preis. Auf der Basis von Sebastian Eiseles Ergebnissen konnte das *ipv* kürzlich neuartige, rückseitenkontaktierte Solarzellen mit einem Wirkungsgrad von über 23,5 % herstellen. Das besondere an diesen High-Tech-Zellen ist eine stark vereinfachte Herstellung, welche eine kostengünstige Produktion erlaubt. Weltweit sind die Forscher an der Universität Stuttgart die Einzigen, welche den High-Tech Prozess beherrschen.

RWE Future Award

Dr. Sebastian Eisele from the *ipv* received the RWE Future Award 2013 for his Ph.D. thesis on laser doping on silicon solar cells. In 2013 dissertations on renewable energies were prized. In this field, Sebastian's fundamental work on laser processes for solar cells was outstanding. Dr. Sebastian Eisele received the award amounting to 13.000 € for his excellent work from Uwe Tigges, member of the managing board of RWE AG. On the basis of Sebastian Eisele's findings, the *ipv* was able to produce a new type of rear-side contacted solar cells with an efficiency over 23.5 %. The characteristic feature of these high-efficiency cells is that their production is much simpler and therefore cheaper compared to conventional solar cells. Throughout the world, the scientists at the University of Stuttgart are the only ones who are proficient in this high-tech process.


Ablauf der Veranstaltung
Begrüßung (Marc Sämann)
Aktuelle Forschung und Entwicklungen am ipv (Jürgen Werner)
Festvortrag: Dr.-Ing. Volker Nadenau
Industrial research @Bosch bridging academia and business
PREISVERLEIHUNG
ipv
Bosch
99
99-01
01-04
04-07
07-08
08-13
13 –
BOSCH

Stuttgarter Photovoltaik Preis des Fördervereins der Freunde des Instituts für Photovoltaik

Der Verein Freunde des Instituts für Photovoltaik (VF*ipv*) zeichnete im November 2014 herausragende studentische Arbeiten im Bereich erneuerbare Energien in vier Kategorien aus. Salvador Regil überzeugte die Jury mit seiner Masterarbeit; in der Kategorie Bachelorarbeit gewann Daniel Wolpert. Sascha Koch wurde für seine Forschungsarbeit ausgezeichnet und für ihre Projektarbeit ging der Preis an das Team Anya Heider, Simon Kostelecky und Maximilian Kraft. Der Förderverein VF*ipv* unterstützt die Forschung in der Photovoltaik und fördert den wissenschaftlichen Nachwuchs.

Die Preisträger 2014 sind:
The 2014 award winners are:

Bachelorarbeit:
Daniel Wolpert

Projektarbeit:
Anya Heider, Simon Kostelecky, Maximilian Kraft

Forschungsarbeit:
Sascha Koch

Masterarbeit:
Salvador E. Martinez Regil

Photovoltaic Award of Stuttgart founded by the nonprofit association "Freunde des Instituts für Photovoltaik"

The nonprofit association "Freunde des Instituts für Photovoltaik" (VF*ipv*) awarded excellent student research projects in the field of renewable energies. Salvador Regil persuaded the jury with his master thesis. Daniel Wolpert won in the category bachelor thesis, Sascha Koch was awarded for his research thesis, and Anya Heider, Simon Kostelecky and Maximilian Kraft for their project work. The VF*ipv* supports research in the field of photovoltaics and promotes young academics.


18. Dezember, ab 17:00 Uhr
SCHLEMMEN mit ISABEL

40-jähriges Dienstjubiläum

Anton Riß feiert 2014 sein 40-jähriges Dienstjubiläum an der Universität Stuttgart. Wir alle am *ipv* gratulieren herzlich!

Isabel Kessler geht in Rente

Nach 12 Jahren am *ipv* verlässt uns Isabel Kessler Ende Dezember 2014 und geht in Rente. Wir wünschen ihr alles Gute für ihren „Unruhestand"!

Isabel Kessler retires

After 12 years at the *ipv* Isabel Kessler leaves us by the end of December 2014 to retire. We wish her all the best for her "(un)restful" retirement.

40th anniversary

Anton Riß celebrates his 40th anniversary at the University of Stuttgart. The *ipv* staff says "Congratulations"!

Mitarbeiterliste

Staff Members

Name	Telefon 0711 - 685 - ...	E-Mail (vorname.name @ipv.uni-stuttgart.de)	Arbeitsgebiet
Leo Bauer	60105	leo.bauer	Technologie-Support
Lydia Beisel	67169	lydia.beisel	Technologie-Support
Marcel Berner	67198	marcel.berner	Optische Charakterisierung
Kai Carstens	67161	kai.carstens	Silizium-Heterostrukturen
Morris Dahlinger	67179	morris.dahlinger	Laserdotieren
Freymut Hilscher	67141	freymut.hilscher	Sekretariat, Verwaltung
Erik Hoffmann	60106	erik.hoffmann	Laser-induzierte Metallisierung
Irmgard Kerschbaum	67158	irmgard.kerschbaum	Buchhaltung
Isabel Kessler	67141	isabel.kessler	Sekretariat, Verwaltung

Jürgen Köhler	67159	juergen.koehler	Personalverwaltung, Gruppenleiter Laserprozesse
Patrick Lill	67171	patrick.lill	Laserdotieren
Brigitte Lutz	67200	brigitte.lutz	Technologie-Support
Hendrik Moldenhauer	67142	hendrik.moldenhauer	Technologie-Support
Kathrin Ohmer	69216	kathrin.ohmer	Laserdotieren
Anton Riß	67214	anton.riss	Werkstatt
Christian Sämann	67178	christian.saemann	Anoden für Li-Ionen-Batterien
Matthias Saueressig	67180	matthias.saueressig	Siebdrucktechnologie
Markus Schubert	67145	markus.schubert	Stellv. Institutsleiter, Gruppenleiter Sensorik

Sergej Vollmer	67201	sergej.vollmer	a-Si-Technologie
Jürgen Werner	67140	juergen.werner	Institutsleiter, Leitung Forschung, Lehre, Verwaltung
Birgitt Winter	67162	birgitt.winter	Gruppenleiterin Technologie
Thomas Wurster	67246	thomas.wurster	Elektronik für die PV
Renate Zapf-Gottwick	69225	renate.zapf-gottwick	Gruppenleiterin Industrielle Solarzellen

Mitarbeiter, ausgeschieden 2013 / 2014

Staff Members who left in 2013 / 2014

Barbara Bazer-Bachi	Hermann Hörth
Alexander Bertram	Jens Kistner
Ahmed Garamoun	Gordana Kulushich
Panagiotis Gedeon	Liv Prönneke
Lars Hamann	Ralph Rothemund
Anja Hardekopf	Tobias Röder
Erika Herrera Calderon	Liviu Stoicescu

Lageplan
Location Plan

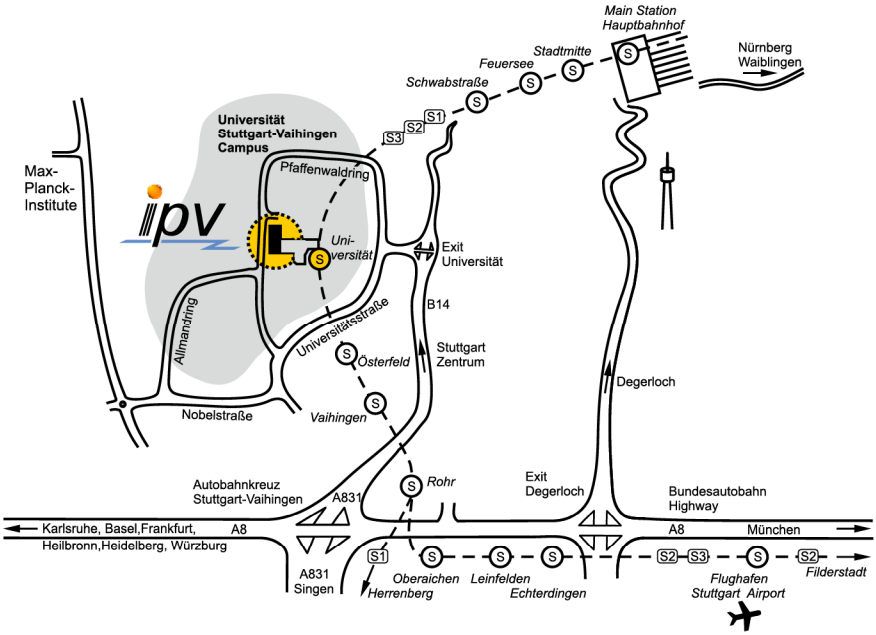

Institut für Photovoltaik
Pfaffenwaldring 47
70569 Stuttgart

Tel.: 0711 / 685-67141

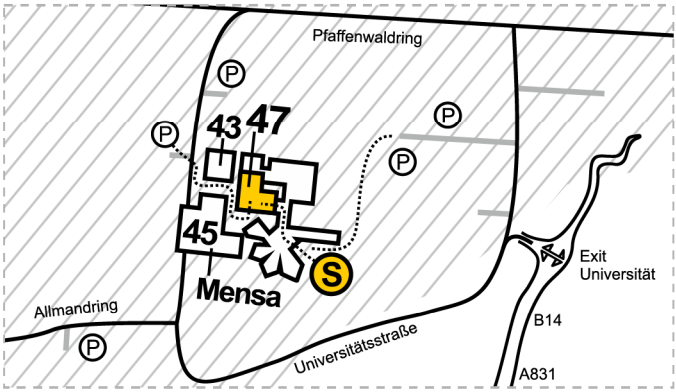

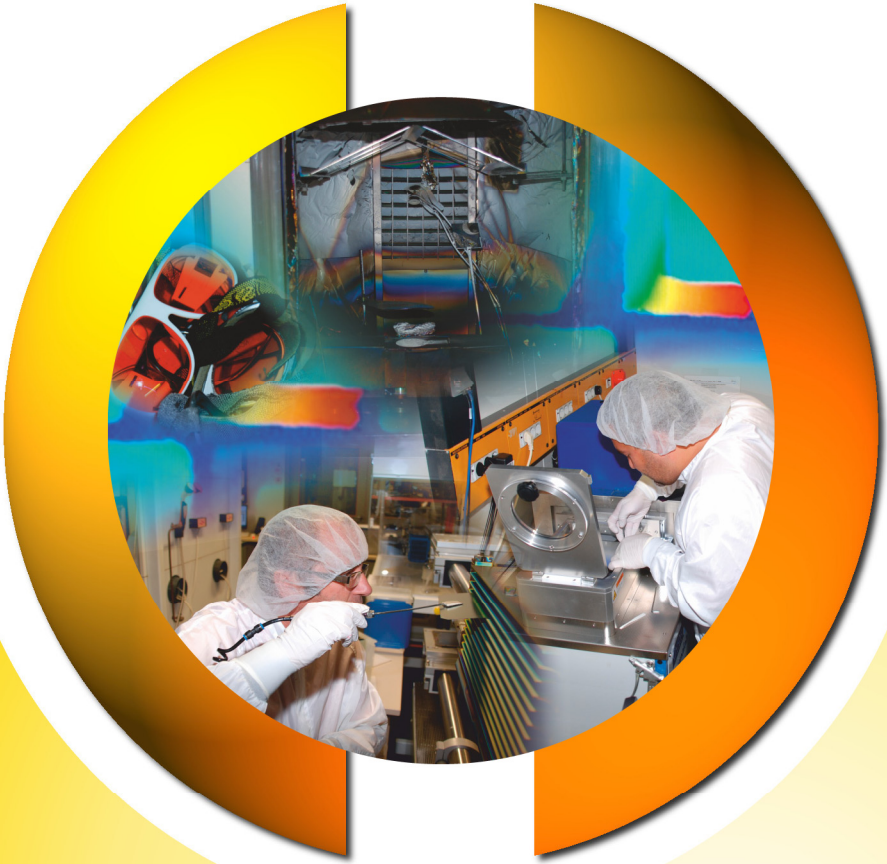

Institut für Photovoltaik
Universität Stuttgart

Pfaffenwaldring 47
70569 Stuttgart

Phone: +49 711 685 67141
FAX: +49 711 685 67143

www.ipv.uni-stuttgart.de